

Ab-initio investigation of transition metal dichalcogenides for the hydrogenation of carbon dioxide to methanol

Avaneesh Balasubramanian ^a, Pawan Kumar Jha ^b, Kaustubh Kaluskar ^c, Sharan Shetty ^c, and
Gopalakrishnan Sai Gautam ^{*b}

^a Indian Institute of Science Education and Research, Pune 411008, India

^b Department of Materials Engineering, Indian Institute of Science, Bengaluru 560012, India

^c Shell India Markets Pvt. Ltd., Bengaluru 562149, India

*E-mail: saigautamg@iisc.ac.in

Abstract

We computationally investigate the catalytic potential of MoSe₂, WS₂, and WSe₂ nanoribbons and nanosheets for the partial hydrogenation of CO₂ to methanol by comparing their electronic, adsorption, and defect properties to MoS₂, a known thermo-catalyst. We identify Se-deficient MoSe₂ (followed by WSe₂) nanosheets to be favorable for selective methanol formation.

Introduction

Transforming CO₂ into valuable chemicals is an effective strategy to reduce anthropogenic CO₂ and promote a circular carbon economy. One way to transform CO₂ is to catalytically convert it into methanol (MeOH), which serves as a precursor for renewable fuels like sustainable aviation fuel and other useful compounds such as formaldehyde [1-6]. However, several catalytic processes to produce MeOH from CO₂ suffer from low conversion and stability or take place at high temperatures making it economically unattractive.

The thermo-catalytic route to convert CO₂ to MeOH has been well studied over the years, with Cu/ZnO being one of the most studied catalytic systems [7]. While the mechanism for the CO₂ conversion on Cu/ZnO is not fully understood, oxygen vacancies on the surface seem to play a significant role [8]. Recently, a study has reported that the in-plane sulphur vacancies of MoS₂ nanosheets are highly selective (94.3% selectivity at 12.5% conversion) towards partial reduction of CO₂ to MeOH at low temperatures, with support from spectroscopic and structural characterization and theoretical calculations [9]. Other transition metal dichalcogenides (TMDC) like MoSe₂, WS₂, and WSe₂ closely resemble MoS₂ in their crystal structures (P6₃/mmc space group), bulk electronic structures, and overall chemistries [10], suggesting the potential of TMDCs besides MoS₂ as potential thermo-catalysts for CO₂ conversion.

For instance, computational and experimental studies on MoSe₂, WS₂, and WSe₂ demonstrate the similarities in the surface activity of these compounds, attributed to the similarities in their electronic structures [11-14]. Additionally, these materials are well-known 2D catalysts, with applications in the hydrogen evolution reaction (HER) [15]. Notably, a recent study [16] has experimentally reported a 93% selectivity at a 9.7% conversion of CO₂ by C-doped MoSe₂ by the thermo-catalytic approach, indicating promising of such TMDCs for

CO₂ conversion. However, detailed insights on the reaction mechanism including computations, which would allow further optimization of such catalysts, was not part of the study [16]. Moreover, to the best of our knowledge, there have been no systematic computational studies comparing and validating the activity of chalcogenide-vacant TMDCs (of composition MX₂ with M = Mo, W and X = S, Se) for CO₂ conversion, motivating this work [6, 17, 18].

In this work, we use density functional theory (DFT) [19, 20] calculations to compare, with MoS₂, the electronic structures, and defective and adsorption energetics of single, double, and triple chalcogenide-vacant TMDC nanosheets and nanoribbons, namely MoSe₂, WS₂ and WSe₂, to explore their potential as catalysts for the partial hydrogenation of CO₂ to MeOH. Since morphology often plays a crucial role in the efficiency of TMDC catalysts [21], we consider all TMDCs in this work to be of nanosheet and nanoribbon morphologies. Specifically, we compute the electronic density of states (DOS), vacancy formation energies, and CO₂ and MeOH adsorption energies for all four TMDCs considered. We compare the calculated properties of MoSe₂, WS₂, and WSe₂ with MoS₂ to examine the similarities and arrive at combinations of candidate material, vacancy content, and morphology that can exhibit partial reduction of CO₂ to a similar extent as MoS₂. While we find all TMDCs considered to exhibit similar qualitative trends in calculated properties compared to MoS₂, we observe in-plane double-Se-vacant MoSe₂ nanosheets (and to an extent, WSe₂ nanosheets) to be the most promising for CO₂ reduction due to its close similarities to the MoS₂ electronic structure, defect, and adsorption energetics. We hope that our work further instigates work in the development of TMDC catalysts for CO₂ reduction.

Structures

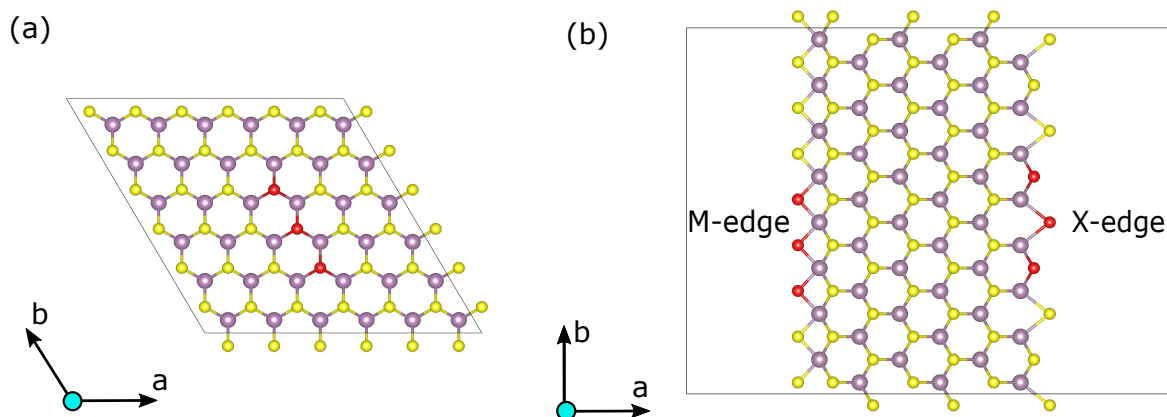


Figure 1: The structures of TMDC nanosheets (panel a) and nanoribbons (panel b), with the yellow and purple spheres denoting X (S,Se) and M (Mo, W) atoms, respectively. Red spheres in both panels denote the X-atoms that are removed sequentially according to their numerical labels to form the single, double and triple vacancies. We consider X-vacancies to form on the in-plane sites of the nanosheets, and at the M- and X-edges of the nanoribbons.

Figure 1 displays the structures used for modelling the nanosheets (panel a) and nanoribbons (panel b) of the TMDCs considered in this work. Nanosheets are single layers with M atoms (purple spheres) arranged in a plane, bonded to X atoms (yellow spheres) ‘above’ and ‘below’ the plane, forming dimers. Following [9], we generate the in-plane vacancies of adjacent X atoms ‘above’ the M-plane of the nanosheets, in the sequence shown by the numerical labels in Figure 1, resulting in single, double, and triple X-vacant nanosheets. In the nanoribbons, the M-edge is formed by capping the M-atoms at the edge with single X atoms in the M-plane, while the X-edge is formed by alternating X dimers and single planar X atoms bonded to M. We generate the X-vacancies on both the M- and X-edges of the nanoribbons sequentially, in accordance with the numerical labels. More details on the structures used is provided in the electronic supporting information (ESI).

Results

Band gaps and defect formation energies

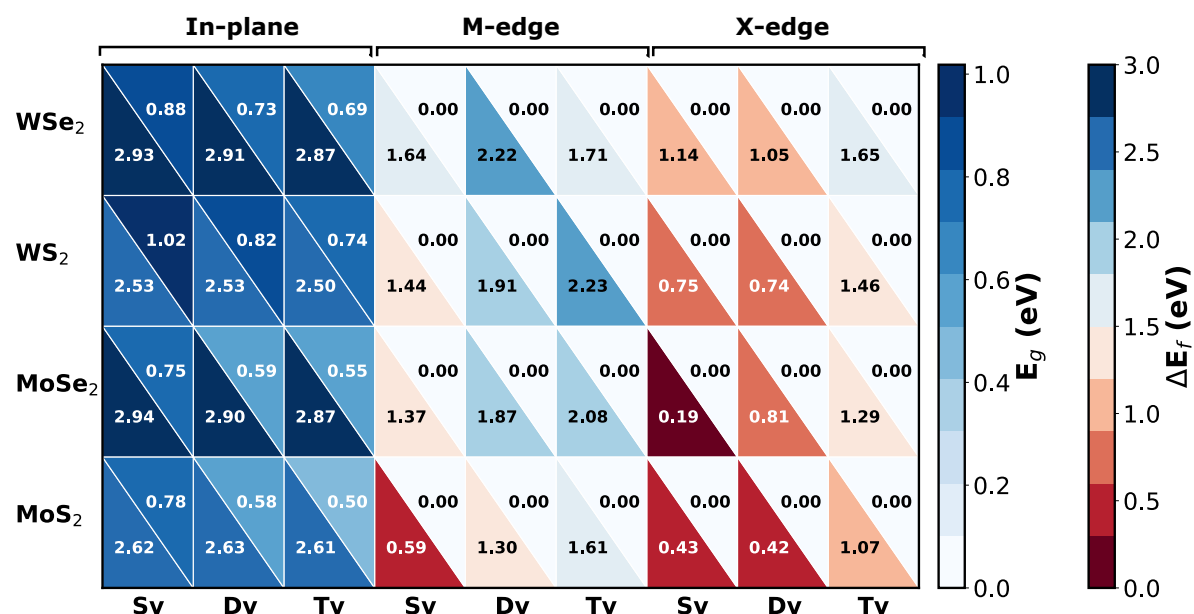


Figure 2: Heatmap of calculated band gaps (E_g) in the upper triangles of each cell and X-vacancy formation energy (ΔE_f) in the lower triangles, for each vacancy at a TMDC. Sv, Dv, and Tv indicate single, double, and triple X-vacant configurations. In-plane refers to nanosheet morphology, while M- and X-edges are part of nanoribbon. ΔE_f are reported in eV per X-vacancy formed.

The catalytic activity of a material is primarily influenced by its electronic structure and the resultant alignment of bands to the electronic states of the reactant [22]. Figure 2 plots the calculated band gap (E_g in eV), based on DOS calculations (see Figures S1-S6 of the ESI) within the upper triangles of each cell for single (Sv), double (Dv), and triple (Tv) X-vacant TMDCs. Metallic states are denoted by white triangles ($E_g = 0$ eV), with dark blue triangles indicating E_g approaching 1 eV. ‘In-plane’ denotes calculations done with the nanosheet morphology while ‘M-edge’ and ‘X-edge’ signify the nanoribbon.

DOS calculations for X-vacant $MoSe_2$, WS_2 , and WSe_2 nanosheets reveal that it lacks electronic states at the Fermi level (i.e., non-metallic), like MoS_2 . Importantly, the E_g of the nanosheets of all TMDCs decrease (by ~ 0.2 - 0.3 eV) as more in-plane X-vacancies are

introduced. X-vacant TMDC nanoribbons, with the X-vacancies at both the M- and X-edges are metallic, similar to our observation in MoS₂ as well (Figure 2 and S5). As observed in [9], the presence of electronic states at the Fermi level in the nanoribbons might hinder the desorption of MeOH formed during hydrogenation from the X-vacant sites, reducing the selectivity of the TMDC nanoribbons towards MeOH release.

Compared to MoSe₂ and WSe₂, the X-vacant WS₂ nanosheets have fewer states/eV at the band edges (Figure S3), suggesting slower kinetics towards CO₂ reduction. Importantly, MoSe₂ exhibits the most similar electronic structure to MoS₂, suggested by the similarities in the calculated DOS for the defective nanosheet configurations (Figure S3) and the resultant E_g only differing by ~ 0.05 eV (Figure 2). This similarity implies that the alignment of the electronic states of in-plane X-vacant MoS₂, which are the most active sites towards MeOH formation from CO₂ [9, 23], towards CO₂ and the reaction intermediates could also be observed for the Se-vacant MoSe₂ nanosheets, making it a possible catalytic candidate. Indeed, the DOS of CO₂ adsorbed at the X-vacant TMDC nanosheets, particularly MoS₂ and MoSe₂ (Figure S6), suggests the alignment of the O p states of CO₂ near the M d -states, which can facilitate the donation of electrons from the d -orbital (HOMO) of the M atoms that are adjacent to X-vacancies to the LUMO of CO₂, facilitating hydrogenation across the C-O bonds.

In addition to electronic structure, the presence of a sufficient number of active sites (the number of X-vacancies in TMDC surfaces and edges in this work) crucially determines a catalyst's effectiveness. To assess the feasibility of generating X-vacancies in pristine nanoribbons and nanosheets, we compute the vacancy formation energies (ΔE_f in eV, lower triangles in Figure 2) for Sv, Dv, and Tv TMDC nanosheets (in-plane) and nanoribbons (M-edge and X-edge). A low (closer to zero or brown triangles in Figure 2) vacancy formation energy indicates a higher equilibrium concentration of X-vacancies at the TMDC surface,

which would result in an increased number of active sites for CO₂ and H₂ binding, thereby enhancing the reaction process and positively impacting the catalytic performance.

As seen in Figure 2, the in-plane S-vacancy ΔE_f on MoS₂ nanosheets are similar to what is reported in [9], with the exception that we find it easier to form S-vacancies at the S-edge than at the Mo-edge in the nanoribbon, which can be attributed to the higher availability of S in the S-edge resulting in easier S-vacancy formation. Like MoS₂, the other TMDCs show lower ΔE_f at the X-edge than at the M-edge as well. The X-vacancy ΔE_f at the in-plane sites of the MoSe₂ and WSe₂ nanosheets are higher than those of MoS₂ (by ~0.25-0.32 eV), with WS₂ showing lower ΔE_f (by 0.1 eV). In case of the nanoribbons, all TMDCs exhibit larger ΔE_f than MoS₂. The higher ΔE_f , especially in MoSe₂ and WSe₂, indicates that the formation of vacancies in these nanoribbons and nanosheets will be less favourable. Given that the in-plane ΔE_f differ by ~0.3 eV in MoSe₂ (and WSe₂) from the corresponding MoS₂ configurations, we can expect a difference in equilibrium concentration of the in-plane vacancies in nanosheets (active sites) to be ~three orders of magnitude at an operating temperature of ~473 K.

CO₂ adsorption energies:

The affinity of the active site(s) towards the reactant (CO₂ here) plays an important role in catalysts' performance. The reactant must bind well to the active site to undergo the reaction and facilitate electron transfer. However, excessive binding could lead to the poisoning of the catalyst's active site. Figure 3 quantifies the CO₂ adsorption energies at different vacancy concentrations (indicated by the colours of each symbol) for the TMDCs considered (signified by shapes of each symbol) in both the nanosheet (in-plane) and nanoribbon (M- and X-edge) morphologies. Since H₂, which is the co-reactant of CO₂ for reduction to MeOH, is a significantly smaller molecule compared to CO₂ and is typically weakly adsorbed (or

physisorbed) at the active sites, we neglect its presence for the calculation of CO₂ adsorption energy. Note that a site with CO₂ adsorption energy that is similar to the active site (in-plane X-vacancies) of MoS₂ is expected to show optimal affinity towards CO₂ for partially hydrogenating it. The CO₂ molecule disintegrates upon adsorption in the Dv M-edge sites of WS₂ and WSe₂, which is why they are not shown in Figure 3.

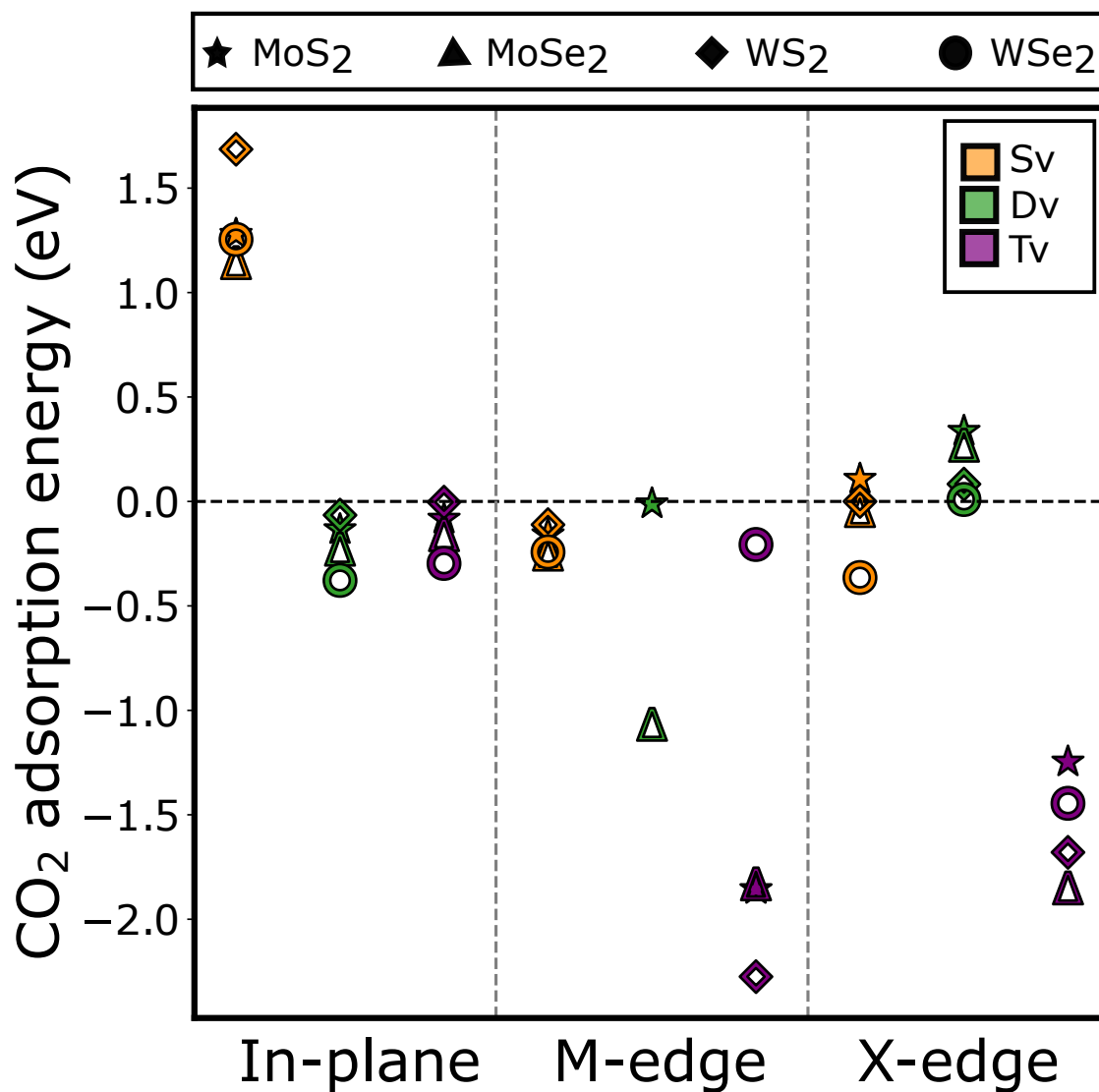


Figure 3: CO₂ adsorption energies in TMDC nanosheets (in-plane) and nanoribbons (M- and X-edge) with X-vacancies. Configurations containing single (Sv), double (Dv), and triple (Tv) vacancies are indicated by orange, green, and purple markers, respectively. Datapoints corresponding to MoS₂, MoSe₂, WS₂, and WSe₂ are indicated by hollow stars, triangles, diamonds, and circles, respectively.

As for the S-vacant MoS₂ nanoribbon, we find that all the Mo-edge sites and triple-S-vacant S-edge sites show negative CO₂ adsorption energies (Figure 3), indicating strong binding. Notably, the X-edge Tv structures show the lowest CO₂ adsorption energies in the corresponding TMDC nanoribbons, indicating excessive binding and potential poisoning of the X-vacant sites. In contrast, CO₂ adsorption is energetically unfavourable on all TMDC nanosheets on the Sv sites, indicating that clustered X-vacancies (i.e., Dv and Tv configurations) are required to kickstart the CO₂ reduction. Similar to MoS₂, we find the adsorption energies of CO₂ to be the lowest (most negative) on Dv sites, among the nanosheets. Therefore, like in MoS₂ [9], an appreciable CO₂ adsorption can also be expected from the other double-X-vacant TMDC nanosheets. Comparing the adsorption energies of the in-plane Dv sites, we find MoSe₂ and WSe₂ sheets to show better CO₂ adsorption than MoS₂ and WS₂.

MeOH adsorption energies:

To verify the ability of TMDC nanosheets and nanoribbons to release MeOH once it is formed and not stay adsorbed and further hydrogenate to methane, we calculate the adsorption energy of MeOH on the X-vacant nanoribbons and nanosheets and plot them in Figure 4. A higher (more positive) adsorption energy implies quick release and therefore higher selectivity to MeOH. From Figure 4, we observe that the adsorption energy of MeOH is higher at the in-plane vacant sheets compared to the M-edge (and X-edge) vacant ribbons for all the TMDC candidates, signifying a higher selectivity towards forming MeOH at the in-plane sites, which is also observed for MoS₂ in [9]. In all the TMDC ribbons, the Dv site shows the lowest MeOH adsorption energy at the M-edge, and the Tv site shows the lowest MeOH adsorption energy at the X-edge. Compared to the in-plane Dv site of MoS₂, the corresponding sites of the other TMDCs show more positive MeOH adsorption energies, with MoSe₂ showing the most

positive value. Hence, among the TMDCs considered, the active site of in-plane Dv of MoSe₂ desorbs MeOH better than MoS₂ and hence should be more selective to MeOH formation and less prone to complete hydrogenation of CO₂ to methane.

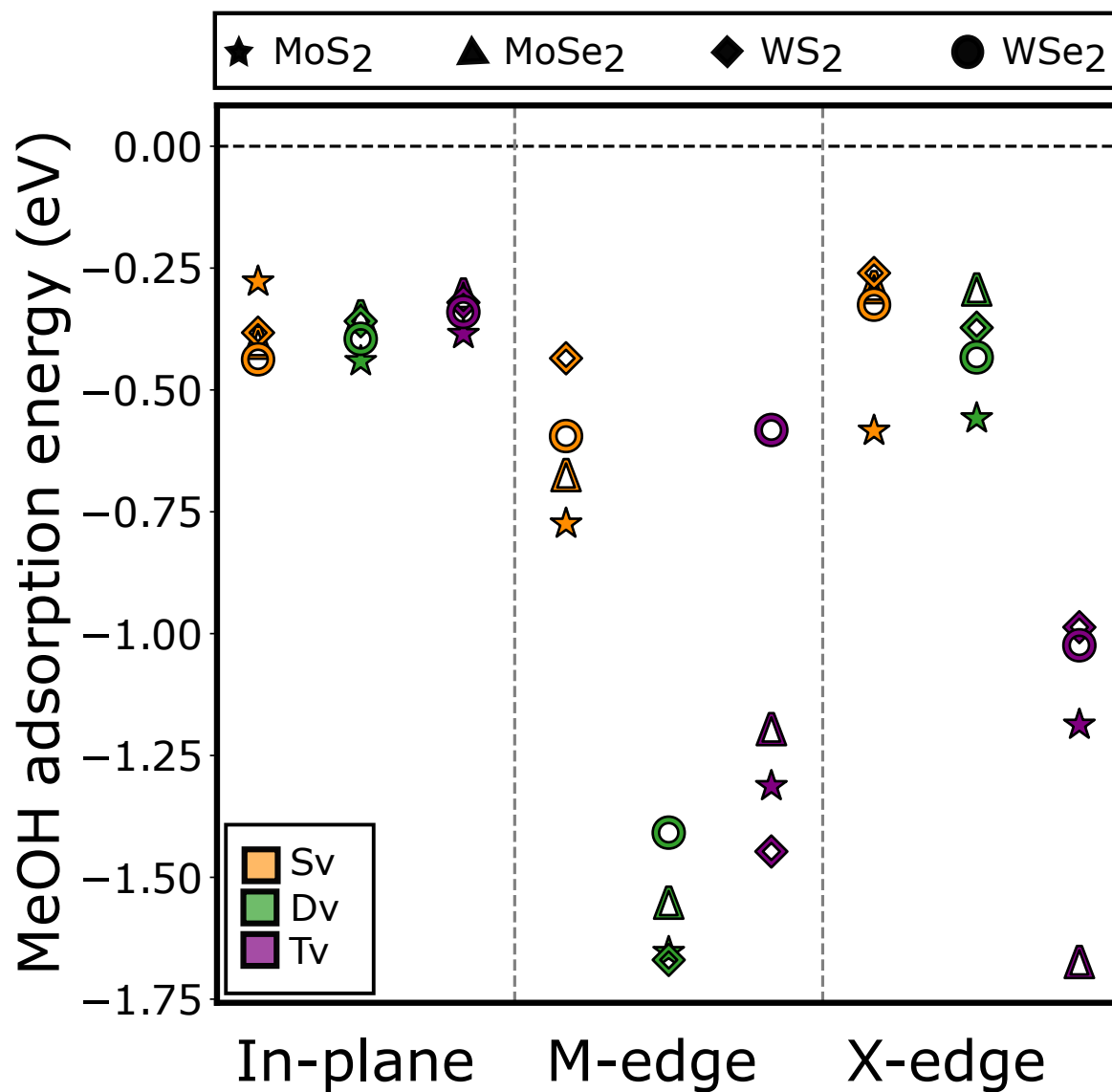


Figure 4: MeOH adsorption energies in X-vacant TMDC nanosheets and nanoribbons considered. Notations in the figure are identical to those used in Figure 3.

Discussion

Our results indicate that the TMDC (MoSe_2 , WS_2 and WSe_2) nanoribbons and nanosheets considered show similar electronic (as seen in the electronic DOS), defect properties (as seen in vacancy ΔE_f) and adsorption thermodynamics (adsorption energies of CO_2 and MeOH) to MoS_2 . However, we find that Se-vacant MoSe_2 nanosheets are the most similar to the S-vacant MoS_2 nanosheets. The similarity between MoSe_2 and MoS_2 can be observed from the similar DOS and E_g of the X-vacant MoSe_2 and MoS_2 structures, better adsorption of CO_2 at the in-plane D_v sites of MoSe_2 and more positive adsorption energies of MeOH at MoSe_2 than at MoS_2 . Since the studies in [9] and [23] suggest that the in-plane vacancies of MoS_2 are the most active sites for partial hydrogenation of CO_2 to MeOH , and we find that the in-plane Se-vacant MoSe_2 show similar properties to those of MoS_2 , we predict MoSe_2 nanosheets to be the most promising candidate among the TMDCs considered for further experimental and computational studies on CO_2 reduction. Additionally, WSe_2 nanosheets are comparable to MoSe_2 in terms of their adsorption energy of CO_2 and relatively higher adsorption energy with MeOH , albeit with larger E_g . Thus, WSe_2 nanosheets can be considered for CO_2 reduction to MeOH as well.

We predict that the M-edge X-vacant nanoribbons would be less selective for MeOH during hydrogenation due to the presence of states at the Fermi level in their electronic structure (Figure S5, which is also reflected in their significant binding of MeOH (Figure 4). While we predict the X-edge X-vacant nanoribbons to be metallic, the presence of states at the Fermi level of these nanoribbons does not necessarily imply poor selectivity towards MeOH , especially in the S_v and D_v configurations. Hence, studies utilising by microkinetic and other experimental adsorption observations are required to ascertain the selectivity of the X-edge of the nanoribbons. However, given the overall electronic structure, defective and adsorption

energetics, we do not expect any of the TMDC nanoribbon morphologies considered in this work to be of significant utility for CO₂ reduction to MeOH.

Conclusion

Utilising anthropogenic CO₂ by transforming it into useful chemicals, fuels, and precursors, such as MeOH, is an important way of ensuring a circular carbon economy. In this study, we used DFT calculations to quantify the electronic structure, vacancy ΔE_f , and CO₂ and MeOH adsorption energies of four TMDCs to explore their utility as thermo-catalysts for CO₂ reduction to MeOH. We considered different concentrations of X-vacancies (S_v, D_v, and T_v) and two different morphologies (nanosheets and nanoribbons) of MoS₂, MoSe₂, WS₂, and WSe₂. Motivated by recent studies [9, 23] that have reported MoS₂ to show a high degree of selectivity for CO₂ conversion to MeOH, we analysed similarities in the calculated properties among the TMDCs to identify potential candidates. Importantly, we found MoSe₂ nanosheets (with D_v of Se) to exhibit E_g , vacancy ΔE_f , and adsorption energies that resemble closest to MoS₂, identifying MoSe₂ to be the most promising among the TMDCs considered, followed by WSe₂. We hope that our work enables the identification of other 2D materials as possible catalysts for selective CO₂ reduction.

Acknowledgment

The authors acknowledge financial support from Shell India Markets Private Limited. The authors gratefully acknowledge the computational resources of the super computer 'PARAM Pravega' provided by Super Computer Education and Research Centre (SERC), IISc. Kaustubh

Kaluskar and Sharan Shetty would like to thank Joost Smits and Sander van Bavel (Shell Global Solutions International B. V.) for fruitful discussions.

Conflicts of interest

There are no conflicts to declare.

Data availability

The computational data supporting this study is openly available at our [GitHub](#) repository.

References

- 1 Adnan, et al., *Green Chem.*, 2021, **23**, 9844.
- 2 M. Ren, et al., *Catalysts*, 2022, **12**, 403.
- 3 T. J. Deka, et al., *Environ. Chem. Lett.*, 2022, **20**, 3525.
- 4 P. Hirunsit, et al., *ACS Sustainable Chem. Eng.*, 2024, **12**, 12143.
- 5 H.-T. Tang, Y.-Z. Pan and Y.-M. Pan, *Green Chem.*, 2023, **25**, 8313.
- 6 Q. Yang and E. V. Kondratenko, in *Advances in CO2 Utilization: From Fundamentals to Applications*, Springer Nature Singapore, 2024, 81.
- 7 S. Kattel, et al., *Science*, 2017, **355**, 1296.
- 8 A. Cao, et al., *ACS Catal.*, 2021, **11**, 1780.
- 9 J. Hu, et al., *Nat. Catal.*, 2021, **4**, 242.
- 10 X. Hu, et al., *Coord. Chem. Rev.*, 2024, **499**, 215504.
- 11 M. Qorbani, et al., *Nat. Commun.*, 2022, **13**, 1256.
- 12 S. Li, et al., *Sep. Purif. Technol.*, 2025, **361**, 131583.
- 13 B. Mahler, et al., *J. Am. Chem. Soc.*, 2014, **136**, 14121.
- 14 B. Kirubasankar, et al., *Chem. Sci.*, 2022, **13**, 7707.
- 15 J. Zhu, et al., *Nat. Commun.*, 2019, **10**, 1348.
- 16 Y. Sun, L. Xiao and W. Wu, *Molecules*, 2024, **29**, 2186.
- 17 K. Stangeland, H. Li and Z. Yu, *Energy Ecol. Environ.*, 2020, **5**, 272.

- 18 Y. Zhang, et al., *Coord. Chem. Rev.*, 2021, **448**, 214147.
- 19 P. Hohenberg and W. Kohn, *Phys. Rev.*, 1964, **136**, B864.
- 20 W. Kohn and L. J. Sham, *Phys. Rev.*, 1965, **140**, A1133.
- 21 S. S. Jakkanawar, et al., *Hydrogen*, 2024, **5**, 776.
- 22 J. R. Kitchin, et al., *J. Chem. Phys.*, 2004, **120**, 10240.
- 23 S. Zhou and H. C. Zeng, *ACS Catal.*, 2022, **12**, 9872.